Global Distribution of the Oceanic Bottom Mixed Layer Thickness

Article *in* Geophysical Research Letters · January 2019

DOI: 10.1029/2018GL081159

5 authors, including:

Peng-Qi Huang
Chinese Academy of Sciences
3 PUBLICATIONS **3** CITATIONS
SEE PROFILE

Xian-Rong Cen
Chinese Academy of Sciences
13 PUBLICATIONS **45** CITATIONS
SEE PROFILE

Yuan-Zheng Lu
Chinese Academy of Sciences
14 PUBLICATIONS **52** CITATIONS
SEE PROFILE

Shuang-Xi Guo
Chinese Academy of Sciences
19 PUBLICATIONS **36** CITATIONS
SEE PROFILE

Geophysical Research Letters

RESEARCH LETTER
10.1029/2018GL081159

Key Points:
- The global distribution of the oceanic bottom mixed layer thickness was assessed with the full-depth WOCE data
- Statistically, the oceanic bottom mixed layer thickness becomes thicker exponentially with depth in the abyssal ocean

Supporting Information:
- Supporting Information S1

Correspondence to:
S.-Q. Zhou,
sqzhou@scsio.ac.cn

Citation:
Huang, P.-Q., Cen, X.-R., Lu, Y.-Z., Guo, S.-X., & Zhou, S.-Q. (2019). Global distribution of the oceanic bottom mixed layer thickness. *Geophysical Research Letters*, *46*. https://doi.org/10.1029/2018GL081159

Received 6 NOV 2018
Accepted 6 JAN 2019
Accepted article online 16 JAN 2019

Global Distribution of the Oceanic Bottom Mixed Layer Thickness

Peng-Qi Huang[1,2], Xian-Rong Cen[1,3], Yuan-Zheng Lu[1,3], Shuang-Xi Guo[1,3], and Sheng-Qi Zhou[1,3]

[1]State Key Laboratory of Tropical Oceanography, South China Sea Institute of Oceanology, Chinese Academy of Sciences, Guangzhou, China, [2]University of Chinese Academy of Sciences, Beijing, China, [3]Institution of South China Sea Ecology and Environmental Engineering, Chinese Academy of Sciences, Guangzhou, China

Abstract The ocean bottom is the Earth's least explored region, and the bottom mixed layer (BML) is the pathway for communication between the ocean interior and the ocean floor. In this study, we used full-depth conductivity-temperature-depth profiles archived by the World Ocean Circulation Experiment Program to obtain the first approximation of the global distribution of the oceanic BML thickness, H_{BML}, by applying an integrated method (Huang, Cen, et al., 2018, https://doi.orag/10.1175/jtech-d-18-0016.1). We found that the median H_{BML} values were 40, 42, and 64 m in the Atlantic, Indian, and Pacific Oceans, respectively, and 47 m globally. Statistically, the peak values for the median H_{BML} were around 20°N or 20°S, and it had weak dependence on the buoyancy frequency, where a thin H_{BML} corresponded to strong stratification. In addition, the median H_{BML} became thicker with the ocean depth (D), according to $H_{BML} = 26.34 + 0.85e^{(D/1271.8)}$.

Plain Language Summary There is an increasing demand in observing the abyssal ocean, the oceanic bottom mixed layer (BML) is the water column communicating with the ocean interior and underlying, where interrelated physical, geochemical, and biological processes actively take place. However, the basic knowledge of the oceanic mixed layer thickness and its spatiotemporal variability is lacking. By using full-depth conductivity-temperature-depth profiles archived by the World Ocean Circulation Experiment Program, we, to the first approximation, show a global distribution of the oceanic BML thickness, with the application of an integrated method. The findings of the oceanic BML thickness in different oceans and its dependencies on latitude and ocean depth would be attractive to various scientific fields.

1. Introduction

The oceanic bottom mixed layer (BML), as shown in the inset of Figure 1, is the part of the water column adjacent to the ocean floor, where active mixing promoted by bottom shear and/or internal wave breaking yields a vertically quasi-homogeneous profile for the temperature, salinity, density, and other properties. The water column is of intrinsic scientific importance in studies of ocean mixing and energy dissipation (McDougall & Ferrari, 2017; Sen et al., 2008; Trowbridge & Lentz, 2018; Wunsch, 1970), the cycling of sediment material, for example (Bianchi et al., 2003), the transport of particulate organic matter (Boudreau & Jorgensen, 2001) and other areas. Moreover, it was stated that the bottom boundary layer must be included in ocean models to properly simulate the overflow of deep water (Killworth, 2003). The BML can be characterized by a couple of parameters, where the thickness of the BML, referred to as H_{BML}, is an important and fundamental parameter. H_{BML} is typically a few tens to hundreds of meters in the oceans (e.g., Armi & Millard, 1976; Weatherly & Martin, 1978) but much smaller in lakes, at only a few meters or less (see literatures in Wüest & Lorke, 2003). In some ocean general circulation models, H_{BML} is set constant as 100 m in high-latitude regions (at latitudes north of 49°N and south of 54°S; Nakano & Suginohara, 2002). However, as suggested by De Lavergne et al. (2016), our basic knowledge of H_{BML} and its spatiotemporal variability are lacking and are in increasing demands in various scientific fields.

In this study, we used an integrated method, developed recently by Huang, Cen, et al. (2018), to identify the BML thickness H_{BML} with the available World Ocean Circulation Experiment (WOCE) data and we characterized the global distribution of H_{BML}. The remainder of this paper is organized as follows. In section 2, we present the hydrographic data, explain the data quality control process, and review the available methods

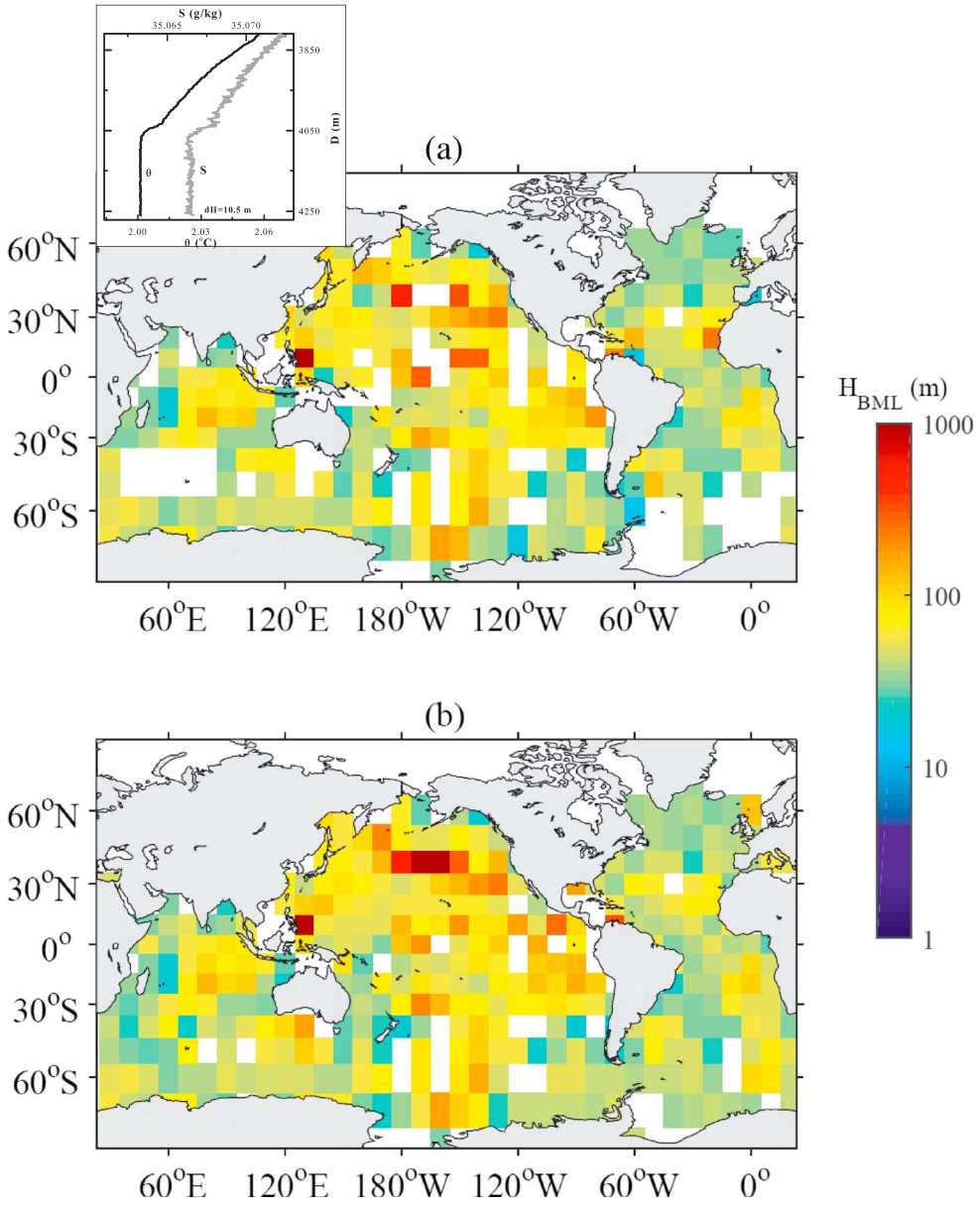

Figure 1. Global maps of BML thickness averaged in 10° × 10° bin. (a) H_{BML} obtained from 12,864 stations where $dH \leq 25$ m and (b) H_{BML1} obtained from 19,119 stations where $dH_1 \leq 25$ m. The inset in (a) shows an example of the BML based on the potential temperature (θ) and salinity (S) profiles measured at station (21.50°N, 21.06°W) along World Ocean Circulation Experiment Section AR21 on 27 April 1998. BML = bottom mixed layer.

for the determination of H_{BML}. In section 3, we describe the global distribution of the BML thickness H_{BML} and discuss its dependence on latitude, buoyancy frequency, and ocean depth. We summarize our findings in section 4.

2. Hydrographical Data and Methodology

We use hydrographical (temperature and salinity) data from the Conductivity-Temperature-Depth (CTD) profilers in the WOCE, Climate Variability and Predictability and other programs, which were downloaded from the websites of Climate Variability and Predictability and Carbon Hydrographic Data Office (https://cchdo.ucsd.edu/) on 9 July 2015. These data were measured along 723 sections and at 34,705 stations from 2 April 1980 to 17 July 2014. The coverage of these stations is shown in Figure 1 of Huang, Lu, et al. (2018).

The data quality was controlled according to the following criteria. (i) The maximum measured CTD depth is set to ≥ 500 m. On the continental shelf, BML might interact with the surface mixed layer, and the dynamics within BML could be more complex due to the influences of wind, internal wave, and other processes. (ii) The mean vertical resolution equals to 1 or 2 m. Following these criteria, some profiles measured in the shallow oceans were removed, and a final data set of 30,152 CTD profiles was left. In the final data set, 80% has the vertical resolution of 2 m. For the CTD data, salinity is typically computed based on temperature and conductivity data and is considerably much more noisy due to the systemic errors, as shown in the inset of Figure 1. The potential density was also affected by the spiky salinity data and it was influenced by the selection of the reference pressure for stations at different ocean depths. Therefore, the potential temperature was used to determine H_{BML} at each station.

The CTD readings in the WOCE database were generally measured over the full ocean depth to the very bottom, thereby providing global coverage and a robust view of the deep water column as well as the BML in regions with varying conditions. In particular, the corrected or uncorrected ocean depths data were provided at 23,154 stations. In general, the CTD profiler was terminated at a certain depth above the sea floor, so the distance from the maximum CTD depth to the ocean bottom (dH) varied among stations. The dH data were available for 15,479 stations, where the dH values were less than 25 m at 12,684 stations. To those stations without dH information, certain procedures (see supporting information) are taken to permit more stations being involved in the BML thickness analysis.

In previous studies, a threshold method, based on the temperature or density profiles, was mainly employed to determine the BML thickness. However, the threshold values vary greatly among different regions (see literatures in Huang, Cen, et al., 2018). In comparison, many studies have aimed to develop methods for accurately computing the oceanic surface mixed layer depth (OSMLD; see literatures in Huang, Lu, et al., 2018). In order to evaluate whether a method can clearly separate the homogeneous mixed layer from the attached strongly stratified water layer, a quality index (QI) was proposed by Lorbacher et al. (2006), subsequently, it was adapted for the BML thickness by Huang, Cen, et al. (2018), which is written as

$$QI = 1 - \frac{\delta_H}{\delta_{1.5\times H}}, \tag{1}$$

where δ_H is the standard deviation of the selected property (temperature,density, etc.) within the BML thickness and $\delta_{1.5\times H}$ is the standard deviation of the property over the depth range from the ocean bottom upward the 1.5 times the BML thickness. Based on the definition of QI, it is expected that QI will approach 1 when the BML is well developed, and the BML thickness can be accurately identified. The QI value will be much less than 1 when the complex structures lie within the mixed layer or a well-developed mixed layer cannot be accurately identified. According to Lorbacher et al. (2006), the mixed layer interpretation is impossible at $QI < 0.5$. This criterion might not be appropriate for the bottom one, considering the QI values of BML are generally lower (Huang, Cen, et al., 2018).

Recently, Huang, Cen, et al. (2018) proposed an integrated method for determining the BML thickness H_{BML}, which was derived from an objective method, the relative variance method, for determining the oceanic surface MLD (Huang, Lu, et al., 2018). In the relative variance method, to any individual temperature (density) profile, a relative variance profile is obtained that is the ratio between the standard deviation and the maximum variation of the temperature (density) from the sea surface, and the depth of the minimum relative variance is defined as the OSMLD. The relative variance method is less dependent on the fixed criteria and its performance is superior to other available methods in the determination of OSMLD in the global ocean (Huang, Lu, et al., 2018). The relative variance method was adapted as an integrated method to determine the BML thickness H_{BML} by additionally considering the results obtained by the threshold, curvature, and maximum angle methods (Chu & Fan, 2011; Lorbacher et al., 2006; Lozovatsky et al., 2008). The integrated method produced the BML thickness values that were consistent with previous observations in most ocean regions. Thus, we employed the integrated method to compute the H_{BML} globally with the available WOCE data. The global distribution of H_{BML} determined by the threshold method is shown for comparison in the supporting information.

3. Distribution of H_{BML}

For the H_{BML} values determined by using the integrated method, it is better to examine its spatial distribution in order to obtain insights of H_{BML}. According to previous observations, the BML thickness remained

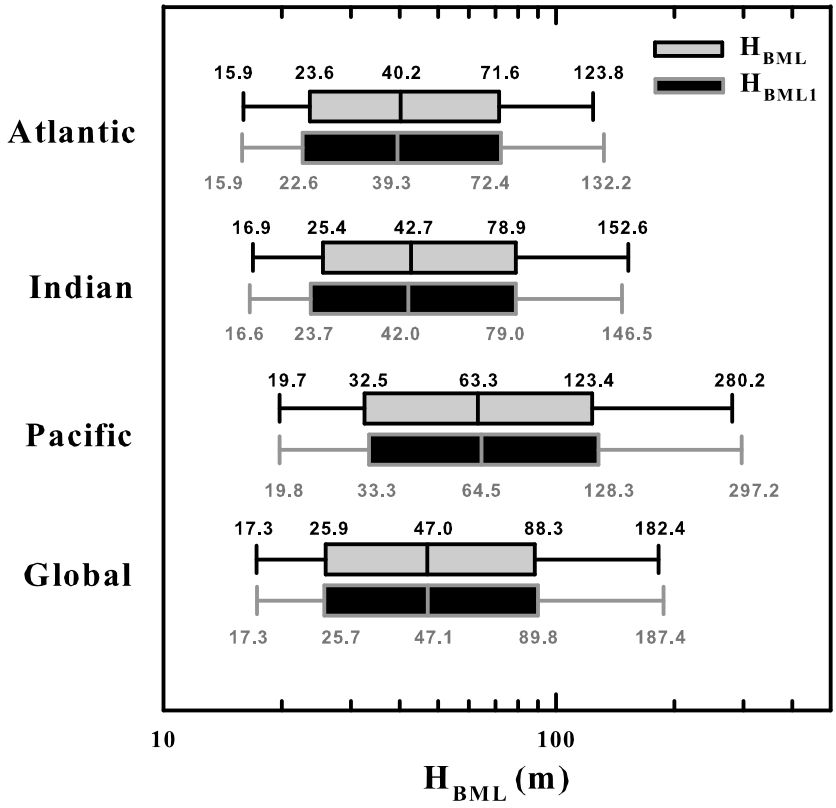

Figure 2. Box-whisker plots of H_{BML} (gray box with black whiskers) and H_{BML1} (black box with gray whiskers) in the Atlantic, Indian, Pacific, and global oceans. In each box-whisker plot, the bar through the box is drawn at the median, the left and right ends of the box are drawn at the quartiles, and the whiskers extend to the tenth and ninetieth percentiles, respectively. The corresponding values are indicated. BML = bottom mixed layer.

relatively steady over a few weeks in the Blake Outer Ridge (Stahr & Sanford, 1999) or even for 1 year in the Canada Basin (Zhou & Lu, 2013). However, H_{BML} exhibits high temporal variability in most regions. For example, in the eastern Atlantic, H_{BML} was less than 10 m on some occasions but greater than 100 m at other times (Saunders & Richards, 1985). Due to the limited coverage of the WOCE data over time, we ignored the temporal variations in the BML thickness in this study. Moreover, the WOCE data were relatively sparse in space, so the H_{BML} values were averaged into $10° \times 10°$ bins. In each bin, the median value was taken when at least 5 H_{BML} values were present, otherwise, it was left blank.

In the WOCE data, the BML could be missed when the CTD cast was terminated at a large dH. Therefore, we only considered the stations where $dH \leq 25$ m for the spatial distribution analysis. However, as shown in Figure 1a, there were many white bins in the global distribution map of H_{BML}, especially in the South Atlantic and Indian Oceans. The ocean depths could alternatively be obtained from the ETOPO1 (1 arc-minute global relief model of Earth's surface) for the ocean bathymetry, the corresponding minimum distance from the bottom was designated as dH_{DE}. By using stations with dH information, the calculated dH_{DE} is very different from the actual value in many cases. However, when the amplitude of dH_{DE} is very small, it was verified that the maximum CTD depth would be very close to the ocean bottom, as explained in the supporting information. Therefore, to those stations without dH information, some of them were included when the amplitude of dH_{DE} was less than 25 m and their dH_{DE} were set as 10 m (the nominal dH value). After including these stations, totally, 19,119 stations could be used, and the corresponding BML thickness was designated as H_{BML1}. As shown in Figure 1, the global distribution of the BML thickness was improved because some white bins were now filled with values.

As shown in Figure 1, H_{BML} exhibited inhomogeneous distributions in different ocean basins. It seems H_{BML} generally becomes thicker around mid-ocean ridges. However, the thickest H_{BML} occurs in the North Pacific Ocean, where coincidently corresponds to the “eddy desert,” a region without any eddy centroid observed

(Chelton et al., 2011). This might provide a clue to find the driving mechanism of such a thick H_{BML}. In the North Atlantic, the median H_{BML} was about 30–40 m, which was consistent with most previous observations (Armi, 1978; Armi & Millard, 1976; Bird et al., 1982; Klein & Mittelstaedt, 1992; Turnewitsch & Springer, 2001). Due to the spatial average, some local observations could not be shown in Figure 1, such as those in Black Ridge and Brazil Basin (Durrieu de Madron & Weatherly, 1994; Stahr & Sanford, 1999). To quantify the variation of H_{BML} in each ocean, box plots were shown in Figure 2. In general, H_{BML} was thinnest in the Atlantic Ocean with a median value of 40 m and a 90% confidence interval of [16, 124] m. In the Indian Ocean, H_{BML} was slightly thicker with a median value of 42 m and a marginally wider 90% confidence interval. H_{BML} was much thicker in the Pacific Ocean, as shown in Figure 1, where the median value was 63 m and the upper bound of the 90% confidence interval was about twice those in the Atlantic and Indian Oceans. The median H_{BML} for the global oceans was 47 m, which was coincidently comparable to the result (46.1 m) obtained based on six WOCE sections in the North Atlantic Ocean (Lozovatsky et al., 2008). This global distribution of H_{BML} would have potential importance in studies of sedimentation and biochemical systems in sea floor. In the global ocean model, the application of a constant H_{BML} (100 m) in high-latitude regions, (e.g., Nakano & Suginohara, 2002), clearly overestimates the BML thickness in most ocean regions and underestimates the BML thickness in other regions. Even when the constant H_{BML} was reduced to small values, for example, 50 m in Yukimoto et al. (2012), the inhomogeneous H_{BML} distribution still had to be considered in ocean models to produce the suitable physical simulations.

4. Dependent Parameters

In previous studies, it was suggested that H_{BML} cannot be precisely defined in terms of a single governing parameter (Armi & Millard, 1976; Perlin et al., 2007; Weatherly & Martin, 1978; Zilitinkevich & Esau, 2002). Thus, using the WOCE data, we examined the relationships between H_{BML} and latitude, ocean depth (D) and buoyancy frequency (N).

Internal tide is one of the most important sources of mechanical energy for mixing. Observations indicate that latitudinal distribution of the mixing rate has a generally symmetrical structure with respect to the equator (Gregg et al., 2003; Tian et al., 2011). Therefore, it is expected that H_{BML} should depend on the latitude. No clear tendency was found based on the scattered H_{BML} distribution at different latitudes. When the zonal average was taken within the latitude of 10° bin, the dependency of H_{BML} on the latitude was determined (Figure 3a). The median H_{BML} was thin in high-latitude regions and it became thicker up to around 20°N or 20°S, before decreasing slightly toward the equatorial region. The trend was similar to that observed in internal tide dissipation (Gregg et al., 2003), which implies that the turbulent diffusion plays an important role in the formation of BML. The median H_{BML} values for the six WOCE sections in the North Atlantic Ocean determined by Lozovatsky et al. (2008) are included in Figure 3a for comparison. The data determined with the threshold method were scattered and their magnitudes differed from those obtained in the present study, but the trends in H_{BML} tendencies in both studies were basically consistent with each other.

In Lozovatsky et al. (2008), it was reported that H_{BML} had no clear dependence on the ocean depth and, on average, H_{BML} was about 1% of the ocean depth in the range of 1,500–5,000 m. Subsequently, Lozovatsky and Shapovalov (2012) showed that a third-degree polynomial could be used to fit the growth of the median H_{BML} with the median ocean depth along the corresponding sections. Using the available WOCE data, we found that H_{BML} became marginally thicker as the ocean depth increased. The dependence of H_{BML} on the depth was clearly demonstrated when H_{BML} was averaged over every depth span of 200 m, as shown in Figure 3b. Considering the ocean depth $D > 1,000$ m, the median H_{BML} could be approximately fitted using the following equation,

$$(H_{BML})_m = 26.34 + 0.85e^{(D/1271.8)}. \quad (2)$$

This equation implies that the median H_{BML} increased exponentially with the ocean depth in the abyssal ocean. When the global ocean depth was averaged to be 3,700 m, the H_{BML} value was deduced to be 42 m, which was slightly thinner than the global median value indicated in Figure 2. When H_{BML} was normalized based on the ocean depth D, the ratio varied over a wide range with a median value of 1.28% and 95% confidence interval of [0.2%, 7.4%].

In previous studies, it was found that the stratification would alter the BML structure and reduce H_{BML} after the comparison between the unstratified turbulent Ekman layer depth and the BML thickness in the field

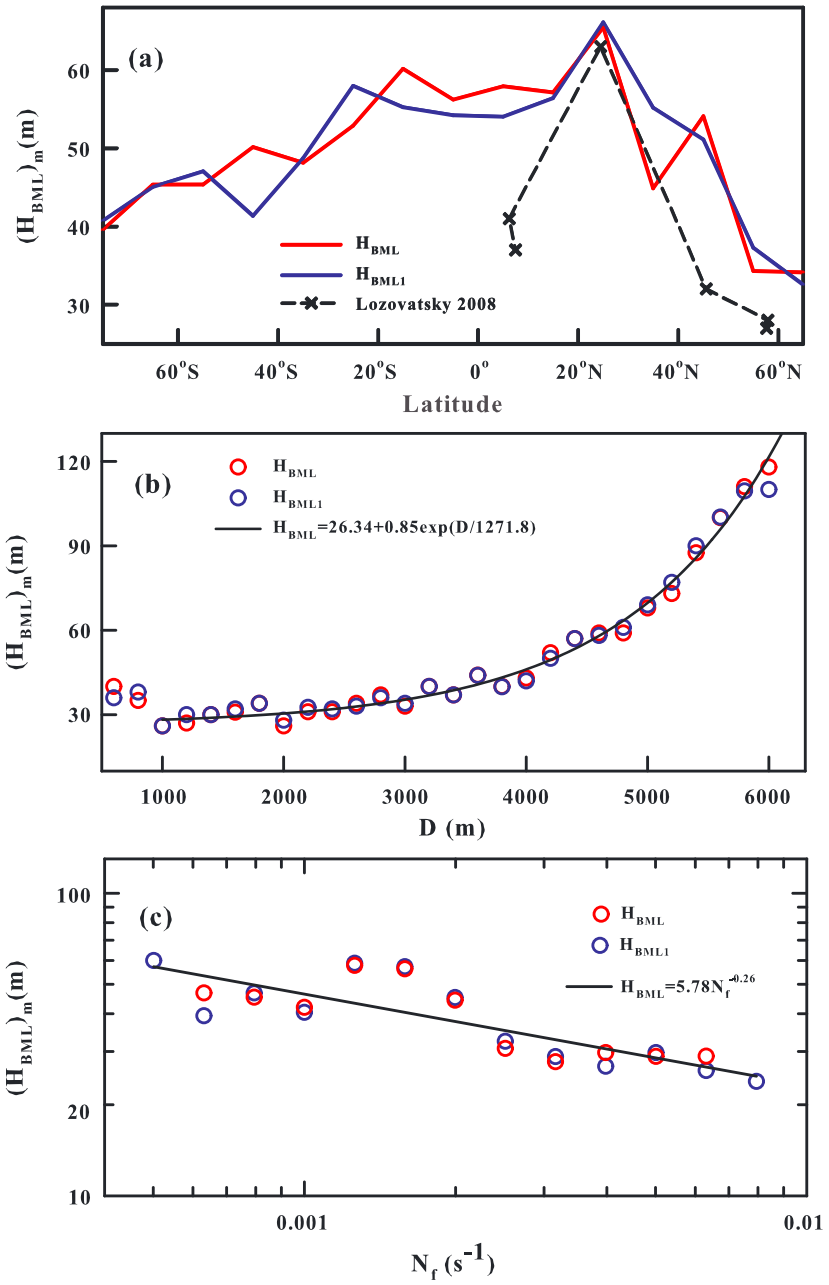

Figure 3. (a) Latitude distribution of the median H_{BML} ($(H_{BML})_m$) binned over 10° in latitude based on H_{BML} (red curve) and H_{BML1} (blue curve). (b) Median H_{BML} as a function of the ocean depth based on H_{BML} (red circles) and H_{BML1} (blue circles). The best fit is plotted as a black curve. (c) Median H_{BML} as a function of buoyancy frequency based on H_{BML} (red circles) and H_{BML1} (blue circles). The best power law fit is plotted as a black curve. BML = bottom mixed layer.

data (Perlin et al., 2007; Pollard et al., 1972; Weatherly & Martin, 1978). Figure 3c shows the median H_{BML} as a function of the buoyancy frequency N_f, where N_f was estimated using the density difference over a depth span of double H_{BML} above the ocean bottom. The results indicated that the median H_{BML} generally became thinner with stronger stratification, although the data were rather scattered. The median H_{BML} data could be fitted with a power law function written as follows

$$(H_{BML})_m = 5.78N_f^{-0.26\pm0.04}. \quad (3)$$

This equations indicated that H_{BML} became smaller as N_f increased, although their dependence was relatively weak. The results in equations (2) and (3) are consistent with each other. It is generally known that

stratifications becomes weaker in the deeper oceans (Becker & Sandwell, 2008), which leads to a thicker H_{BML} according to either equations (2) or (3). The dependency of H_{BML} on the buoyancy frequency N_f appeared to be less clear than that on the depth D. This result might imply that other factors, except for the buoyancy frequency N_f, should be considered to obtain a better understanding on H_{BML}. However, the effects of other factors, such as roughness and geothermal heating, on H_{BML} could not be resolved with the current data set, which may suggest that these factors are less dominant or more observation data is needed.

5. Summary and Discussion

In this study, we used full-depth CTD profiles from the WOCE program to evaluate the global distribution of the BML thickness H_{BML}. H_{BML} was computed with a recently proposed integrated method, which was examined to be superior to other available methods. H_{BML} had an inhomogeneous distributions in different ocean basins and appeared thicker around mid-ocean ridges. In particular, the median H_{BML} values were determined as 40, 42, and 64 m in the Atlantic, Indian, and Pacific Oceans, respectively. Globally, the median H_{BML} value was 47 m, which is thinner than that used in some ocean models. Using a rather limited amount of the full-depth CTD data, we found that the Ekman theory could not fully describe H_{BML} depending on the latitude. H_{BML} had maximum values around 20°N or 20°S, which are similar to those observed in inertial tide dissipation. The stratification appeared to reduce H_{BML} based on the weak dependence of H_{BML} on the buoyancy frequency N_f ($(H_{BML})_m = 5.78N_f^{-0.26\pm0.04}$). In the abyssal ocean ($D > 1,000$ m), H_{BML} became thicker in the deeper ocean, and it could be statistically fitted by an exponential function of $(H_{BML})_m = 26.34 + 0.85e^{(D/1271.8)}$. Alternatively, H_{BML} was about 1.28% of the ocean depth. This study is the first to provide an overview of the global distribution of H_{BML}, but more precise field measurements are needed to fully understand the global dynamics of BML.

Acknowledgments
This study was supported by the National Natural Science Foundation of China (91752108, 41476167, 41776033, and 41706029), the National Natural Science Foundation of Guangdong Province, China (2016A030311042), Guangzhou Science and Technology Program key project (201804020056), and the Research Programs of the Chinese Academy of Sciences (XDA11030302 and ISEE2018PY05). We also thank those who helped to collect, calibrate, process, and archive the WOCE, CLIVAR, and GO-SHIP hydrographic section data. The data used in this study can be downloaded from https://cchdo.ucsd.edu/.

References

Armi, L. (1978). Some evidence for boundary mixing in the deep ocean. *Journal of Geophysical Research*, *83*(C4), 1971–1979.
Armi, L., & Millard, R. C. (1976). The bottom boundary layer of the deep ocean. *Journal of Geophysical Research*, *81*, 4983–4990.
Becker, J. J., & Sandwell, D. T. (2008). Global estimates of seafloor slope from single-beam ship soundings. *Journal of Geophysical Research*, *113*, C05028. https://doi.org/10.1029/2006JC003879
Bianchi, A., Tholosan, O., Garcin, J., Polychronaki, T., Tselepides, A., Buscail, R., & Duineveld, G. (2003). Microbial activities at the benthic boundary layer in the Aegean Sea. *Progress in Oceanography*, *57*(2), 219–236.
Bird, A. A., Weatherly, G. L., & Wimbush, M. (1982). A study of the bottom boundary layer over the eastward scarp of the Bermuda Rise. *Journal of Geophysical Research*, *87*(C10), 7941–7954.
Boudreau, B. P., & Jorgensen, B. B. (2001). *The benthic boundary layer: Transport processes and biogeochemistry*. Oxford, New York: Oxford University Press.
Chelton, D. B., Schlax, M. G., & Samelson, R. M. (2011). Global observations of nonlinear mesoscale eddies. *Progress in Oceanography*, *91*(2), 167–216.
Chu, P. C., & Fan, C. (2011). Maximum angle method for determining mixed layer depth from seaglider data. *Journal of the Oceanographical*, *67*(2), 219–230.
De Lavergne, C., Madec, G., Capet, X., Maze, G., & Roquet, F. (2016). Getting to the bottom of the ocean. *Nature Geoscience*, *9*(12), 857–858.
Durrieu de Madron, X., & Weatherly, G. (1994). Circulation, transport and bottom boundary layers of the deep currents in the Brazil Basin. *Journal of Marine Research*, *52*(4), 583–638.
Gregg, M. C., Sanford, T. B., & Winkel, D. P. (2003). Reduced mixing from the breaking of internal waves in equatorial waters. *Nature*, *422*(6931), 513–515.
Huang, P.-Q., Cen, X.-R., Lu, Y.-Z., Guo, S.-X., & Zhou, S.-Q. (2018). An integrated method for determining the oceanic bottom mixed layer thickness based on WOCE potential temperature profiles. *Journal of Atmospheric and Oceanic Technology*, *35*(11), 2289–2301. https://doi.org/10.1175/jtech-d-18-0016.1
Huang, P.-Q., Lu, Y.-Z., & Zhou, S.-Q. (2018). An objective method for determining ocean mixed layer depth with applications to WOCE data. *Journal of Atmospheric and Oceanic Technology*, *35*(3), 441–458.
Killworth, P. D. (2003). Inclusion of the bottom boundary layer in ocean models. In P. Muller (Ed.), *Proceedings of the 13th' Aha Huliko'a Hawaiian Winter Workshop on Near Boundary Processes and their Parameterization* (pp. 177–185). Honolulu, HI: University of Hawaii SOEST.
Klein, H., & Mittelstaedt, E. (1992). Currents and dispersion in the abyssal Northeast Atlantic. Results from the NOAMP field program. *Deep Sea Research Part A. Oceanographic Research Papers*, *39*(10), 1727–1745.
Lorbacher, K., Dommenget, D., Niiler, P., & Köhl, A. (2006). Ocean mixed layer depth: A subsurface proxy of ocean-atmosphere variability. *Journal of Geophysical Research*, *111*, C07010. https://doi.org/10.1029/2003JC002157
Lozovatsky, I., Fernando, H., & Shapovalov, S. (2008). Deep-ocean mixing on the basin scale: Inference from North Atlantic transects. *Deep Sea Research Part I: Oceanographic Research Papers*, *55*(9), 1075–1089.
Lozovatsky, I., & Shapovalov, S. (2012). Thickness of the mixed bottom layer in the Northern Atlantic. *Oceanology*, *52*(4), 447–452.
McDougall, T. J., & Ferrari, R. (2017). Abyssal upwelling and downwelling driven by near-boundary mixing. *Journal of Physical Oceanography*, *47*(2), 261–283.
Nakano, H., & Suginohara, N. (2002). Effects of bottom boundary layer parameterization on reproducing deep and bottom waters in a world ocean model. *Journal of Physical Oceanography*, *32*(4), 1209–1227.

Perlin, A., Moum, J., Klymak, J., Levine, M., Boyd, T., & Kosro, P. (2007). Organization of stratification, turbulence, and veering in bottom Ekman layers. *Journal of Geophysical Research*, *112*, 12. https://doi.org/10.1029/2004JC002641

Pollard, R. T., Rhines, P. B., & Thompson, R. O. (1972). The deepening of the wind-mixed layer. *Geophysical & Astrophysical Fluid Dynamics*, *4*(1), 381–404.

Saunders, P., & Richards, K. (1985). Benthic boundary layer-IOS Observational and Modelling Programme: Final report. january, 1985.

Sen, A., Scott, R. B., & Arbic, B. K. (2008). Global energy dissipation rate of deep-ocean low-frequency flows by quadratic bottom boundary layer drag: Computations from current-meter data. *Geophysical Research Letters*, *35*, L09606. https://doi.org/10.1029/2008GL033407

Stahr, F. R., & Sanford, T. B. (1999). Transport and bottom boundary layer observations of the North Atlantic Deep Western Boundary Current at the Blake Outer Ridge. *Deep Sea Research Part II: Topical Studies in Oceanography*, *46*(1), 205–243.

Tian, J.-W., Zhou, L., & Zhang, X.-Q. (2011). Latitudinal distribution of mixing rate caused by the M2 internal tide. *Journal of Physical Oceanography*, *36*, 35–42. https://doi.org/10.1175/JPO2824.1

Trowbridge, J. H., & Lentz, S. J. (2018). The bottom boundary layer. *Annual Review of Marine Science*, *10*(1), 397–420.

Turnewitsch, R., & Springer, B. M. (2001). Do bottom mixed layers influence 234th dynamics in the abyssal near-bottom water column? *Deep Sea Research Part I: Oceanographic Research Papers*, *48*(5), 1279–1307.

Weatherly, G. L., & Martin, P. J. (1978). On the structure and dynamics of the oceanic bottom boundary layer. *Journal of Physical Oceanography*, *8*(4), 557–570.

Wüest, A., & Lorke, A. (2003). Small-scale hydrodynamics in lakes. *Annual Review of fluid mechanics*, *35*(1), 373–412.

Wunsch, C. (1970). On oceanic boundary mixing. *Deep Sea Research*, *17*, 293–301.

Yukimoto, S., Adachi, Y., Hosaka, M., Sakami, T., Yoshimura, H., & Hirabara, M. (2012). A new global climate model of the meteorological research institute: MRI-CGCM3 model description and basic performance. *Journal of the Meteorological Society of Japan*, *90*(2), 23–64.

Zhou, S.-Q., & Lu, Y.-Z. (2013). Characterization of double diffusive convection steps and heat budget in the deep Arctic Ocean. *Journal of Geophysical Research: Oceans*, *118*, 6672–6686. https://doi.org/10.1002/2013JC009141

Zilitinkevich, S., & Esau, I. (2002). On integral measures of the neutral barotropic planetary boundary layer. *Boundary-Layer Meteorology*, *104*(3), 371–379.